Towards Efficient Training and Evaluation of Robust Models against l_0 Bounded Adversarial Perturbations

Xuyang Zhong[1] Yixiao Huang[1 2] Chen Liu[1]

Abstract

This work studies sparse adversarial perturbations bounded by l_0 norm. We propose a white-box PGD-like attack method named sparse-PGD to effectively and efficiently generate such perturbations. Furthermore, we combine sparse-PGD with a black-box attack to comprehensively and more reliably evaluate the models' robustness against l_0 bounded adversarial perturbations. Moreover, the efficiency of sparse-PGD enables us to conduct adversarial training to build robust models against sparse perturbations. Extensive experiments demonstrate that our proposed attack algorithm exhibits strong performance in different scenarios. More importantly, compared with other robust models, our adversarially trained model demonstrates state-of-the-art robustness against various sparse attacks. Codes are available at https://github.com/CityU-MLO/sPGD.

1. Introduction

Deep learning has been developing tremendously fast in the last decade. However, it is shown vulnerable to adversarial attacks: imperceivable adversarial perturbations (Szegedy et al., 2013; Kurakin et al., 2016) could change the prediction of a model without altering the input's semantic content, which poses great challenges in safety-critical systems. Among different kinds of adversarial perturbations, the ones bounded by l_∞ or l_2 norms are mostly well-studied (Goodfellow et al., 2014; Madry et al., 2017; Zhang et al., 2019c) and benchmarked (Croce et al., 2020), because these adversarial budgets, i.e., the sets of all allowable perturbations, are convex, which facilitates theoretical analyses and algorithm design. By contrast, we study perturbations bounded by l_0 norm in this work. These perturbations are sparse and quite common in physical scenarios, including broken pixels in LED screens to fool object detection models and adversarial stickers on road signs to make an auto-driving system fail (Papernot et al., 2017; Akhtar & Mian, 2018; Xu et al., 2019; Feng et al., 2022; Wei et al., 2023).

However, constructing l_0 bounded adversarial perturbations is challenging as the corresponding adversarial budget is non-convex. Therefore, gradient-based methods, such as projected gradient descent (PGD) (Madry et al., 2017), usually cannot efficiently obtain a strong adversarial perturbation. In this regard, existing methods to generate sparse perturbations (Modas et al., 2018; Croce & Hein, 2019b; Su et al., 2019; Dong et al., 2020; Croce et al., 2022) either cannot control the l_0 norm of perturbations or have prohibitively high computational complexity, which makes them inapplicable for adversarial training to obtain robust models against sparse perturbations. The perturbations bounded by l_1 norm are the closest scenario to sparse perturbations among convex adversarial budgets defined by an l_p norm. Nevertheless, adversarial training in this case (Tramer & Boneh, 2019; Croce & Hein, 2021) still suffers from issues such as slow convergence and instability. Jiang et al. (2023) demonstrates that these issues arise from non-sparse perturbations bounded by l_1 norm. In other words, l_1 adversarial budget still cannot guarantee the sparsity of the perturbations. Thus, it is necessary to study the case of l_0 bounded perturbations.

In this work, we propose a white-box attack named sparse-PGD (sPGD) to effectively and efficiently generate sparse perturbations bounded by l_0 norm. Specifically, we decompose the sparse perturbation $\boldsymbol{\delta}$ as the product of a magnitude tensor $\boldsymbol{p}$ and a binary sparse mask $\boldsymbol{m}$: $\boldsymbol{\delta} = \boldsymbol{p} \odot \boldsymbol{m}$, where $\boldsymbol{p}$ and $\boldsymbol{m}$ determine the magnitudes and the locations of perturbed features, respectively. We adopt PGD-like algorithms to update $\boldsymbol{p}$ and $\boldsymbol{m}$. However, it is challenging to directly optimize the binary mask $\boldsymbol{m}$ in the discrete space. We thereby introduce an alternative continuous variable $\widetilde{\boldsymbol{m}}$ to approximate $\boldsymbol{m}$ and update $\widetilde{\boldsymbol{m}}$ by gradient-based methods, $\widetilde{\boldsymbol{m}}$ is then transformed to $\boldsymbol{m}$ by projection to the discrete space. Due to the sparsity of $\boldsymbol{m}$ by the projection operator, the gradient of $\boldsymbol{p}$ is sparse, which may lead to slow convergence by coordinate descent. Therefore, we can remove

[1] City University of Hong Kong, Hong Kong SAR, China [2] University of Michigan, Ann Arbor, USA. Correspondence to: Chen Liu <chen.liu@cityu.edu.hk>, Xuyang Zhong <xuyang.zhong@my.cityu.edu.hk>.

Proceedings of the 41^{st} International Conference on Machine Learning, Vienna, Austria. PMLR 235, 2024. Copyright 2024 by the author(s).

the projection operator in the backpropagation to obtain the unprojected gradient of $\boldsymbol{p}$. We use both the original sparse gradient and the unprojected gradient of $\boldsymbol{p}$ to boost the attack performance. Moreover, we design a random reinitialization mechanism to enhance the exploration capability for the mask $\boldsymbol{m}$. On top of sPGD, we propose sparse-AutoAttack (sAA), which is the ensemble of the white-box sPGD and another black-box sparse attack, for a more comprehensive and reliable evaluation against l_0 bounded perturbations. Through extensive experiments, we show that our method exhibits better performance than other attacks.

More importantly, we explore adversarial training to obtain robust models against sparse attacks. In this context, the attack method will be called in each mini-batch update, so it should be both effective and efficient. Compared with existing methods, our proposed sPGD performs much better when using a small number of iterations, making it feasible for adversarial training and its variants (Zhang et al., 2019b). Empirically, models adversarially trained by sPGD demonstrate the strongest robustness against various sparse attacks.

We summarize the contributions of this paper as follows:

1. We propose an effective and efficient white-box attack algorithm named sparse-PGD (sPGD) to generate l_0 bounded adversarial perturbations.
2. sPGD achieves the best performance among white-box sparse attacks. We then combine it with a black-box sparse attack to construct sparse-AutoAttack (sAA) for more comprehensive robustness evaluation against l_0 bounded adversarial perturbations.
3. sPGD achieves much better performance in the regime of limited iterations, it is then adopted for adversarial training. Extensive experiments demonstrate that models adversarially trained by sPGD have significantly stronger robustness against various sparse attacks.

2. Preliminaries

We use image classification as an example, although the proposed methods are applicable to any classification model. Under l_p bounded perturbations, the robust learning aims to solve the following min-max optimization problem.

$$\begin{gathered}\min_{\boldsymbol{\theta}} \frac{1}{N}\sum_{i=1}^{N}\max_{\boldsymbol{\delta}_i}\mathcal{L}(\boldsymbol{\theta}, \boldsymbol{x}_i+\boldsymbol{\delta}_i), \\ \text{s.t. } ||\boldsymbol{\delta}_i||_p \leq \epsilon,\ 0 \leq \boldsymbol{x}_i+\boldsymbol{\delta}_i \leq 1.\end{gathered} \tag{1}$$

where $\boldsymbol{\theta}$ denotes the parameters of the model and $\mathcal{L}$ is the loss objective function. $\boldsymbol{x}_i \in \mathbb{R}^{h\times w\times c}$ is the input image where h, w and c represent the height, width, and number of channels, respectively. $\boldsymbol{\delta}_i$ has the same shape as $\boldsymbol{x}_i$ and represents the perturbation. The perturbations are constrained by its l_p norm and the bounding box. In this regard, we use the term *adversarial budget* to represent the set of all allowable perturbations. Adversarial attacks focus on the inner maximization problem of (1) and aim to find the optimal adversarial perturbation, while adversarial training focuses on the outer minimization problem of (1) and aims to find a robust model parameterized by $\boldsymbol{\theta}$. Due to the high dimensionality and non-convexity of the loss function when training a deep neural network, (Weng et al., 2018) has proven that solving the problem (1) is at least NP-complete.

We consider the pixel sparsity for image inputs in this work, which is more meaningful than feature sparsity and consistent with existing works (Croce & Hein, 2019b; Croce et al., 2022). That is, a pixel is considered perturbed if *any* of its channel is perturbed, and sparse perturbation means few pixels are perturbed.

3. Related Works

Non-Sparse Attacks: The pioneering work (Szegedy et al., 2013) finds the adversarial perturbations to fool image classifiers and proposes a method to minimize the l_2 norm of such perturbations. To more efficiently generate adversarial perturbations, the fast gradient sign method (FGSM) (Goodfellow et al., 2014) generates l_∞ perturbation in one step, but its performance is significantly surpassed by the multi-step variants (Kurakin et al., 2017). Projected Gradient Descent (PGD) (Madry et al., 2017) further boosts the attack performance by using iterative updating and random initialization. Specifically, each iteration of PGD updates the adversarial perturbation $\boldsymbol{\delta}$ by:

$$\boldsymbol{\delta} \longleftarrow \Pi_{\mathcal{S}}(\boldsymbol{\delta} + \alpha \cdot s(\nabla_{\boldsymbol{\delta}}\mathcal{L}(\boldsymbol{\theta}, \boldsymbol{x}+\boldsymbol{\delta}))) \tag{2}$$

where $\mathcal{S}$ is the adversarial budget, α is the step size, $s : \mathbb{R}^{h\times w\times c} \rightarrow \mathbb{R}^{h\times w\times c}$ selects the steepest ascent direction based on the gradient of the loss $\mathcal{L}$ with respect to the perturbation. Inspired by the first-order Taylor expansion, Madry et al. (2017) derives the steepest ascent direction for l_2 bounded and l_∞ bounded perturbations to efficiently find strong adversarial examples; SLIDE (Tramer & Boneh, 2019) and l_1-APGD (Croce & Hein, 2021) use k-coordinate ascent to construct l_1 bounded perturbations, which is shown to suffer from the slow convergence (Jiang et al., 2023).

Besides the attacks that have access to the gradient of the input (i.e., white-box attacks), there are black-box attacks that do not have access to model parameters, including the ones based on gradient estimation through finite differences (Bhagoji et al., 2018; Ilyas et al., 2018a;b; Tu et al., 2018; Uesato et al., 2018) and the ones based on evolutionary strategies or random search (Alzantot et al., 2018; Guo et al., 2019). To improve the query efficiency of these attacks, (Al-Dujaili & O'Reilly, 2019; Moon et al., 2019; Meunier et al., 2019; Andriushchenko et al., 2019) generate adversarial perturbation at the corners of the adversarial budget.

To more reliably evaluate the robustness, Croce & Hein (2020) proposes AutoAttack (AA) which consists of an ensemble of several attack methods, including both black-box and white-box attacks. Croce & Hein (2021) extends AA to the case of l_1 bounded perturbations and proposes AutoAttack-l_1 (AA-l_1). Although the l_1 bounded perturbations are usually sparse, Jiang et al. (2023) demonstrates that AA-l_1 is able to find non-sparse perturbations that cannot be found by SLIDE to fool the models. That is to say, l_1 bounded adversarial perturbations are not guaranteed to be sparse. We should study perturbations bounded by l_0 norm.

Sparse Attacks: For perturbations bounded by l_0 norm, directly adopting vanilla PGD as in Eq. (2) leads to suboptimal performance due to the non-convexity nature of the adversarial budget: PGD_0 (Croce & Hein, 2019b), which updates the perturbation by gradient ascent and project it back to the adversarial budget, turns out very likely to trap in the local maxima. Different from PGD_0, CW L0 (Carlini & Wagner, 2017) projects the perturbation onto the feasible set based on the absolute product of gradient and perturbation and adopts a mechanism similar to CW L2 (Carlini & Wagner, 2017) to update the perturbation. SparseFool (Modas et al., 2018) and GreedyFool (Dong et al., 2020) also generate sparse perturbations, but they do not strictly restrict the l_0 norm of perturbations. If we project their generated perturbations to the desired l_0 ball, their performance will drastically drop. Sparse Adversarial and Interpretable Attack Framework (SAIF) (Imtiaz et al., 2022) is similar to our method in that SAIF also decomposes the l_0 perturbation into a magnitude tensor and sparsity mask, but it uses the Frank-Wolfe algorithm (Frank et al., 1956) to separately update them. SAIF turns out to get trapped in local minima and shows poor performance on adversarially trained models. Besides white-box attacks, there are black-box attacks to generate sparse adversarial perturbations, including CornerSearch (Croce & Hein, 2019b) and Sparse-RS (Croce et al., 2022). However, these black-box attacks usually require thousands of queries to find an adversarial example, making it difficult to scale up to large datasets.

Adversarial Training: Despite the difficulty in obtaining robust deep neural network, adversarial training (Madry et al., 2017; Croce & Hein, 2019a; Sehwag et al., 2021; Rebuffi et al., 2021; Gowal et al., 2021; Rade & Moosavi-Dezfooli, 2021; Cui et al., 2023; Wang et al., 2023) stands out as a reliable and popular approach to do so (Athalye et al., 2018; Croce & Hein, 2020). It generates adversarial examples first and then uses them to optimize model parameters. Despite effective, adversarial training is time-consuming due to multi-step attacks. Shafahi et al. (2019); Zhang et al. (2019a); Wong et al. (2020); Sriramanan et al. (2021) use weaker but faster one-step attacks to reduce the overhead, but they may suffer from catastrophic overfitting (Kang & Moosavi-Dezfooli, 2021): the model overfits to these weak attacks during training instead of achieving true robustness to various attacks. Kim et al. (2020); Andriushchenko & Flammarion (2020); Golgooni et al. (2021); de Jorge et al. (2022) try to overcome catastrophic overfitting while maintaining efficiency.

Compared with l_∞ and l_2 bounded perturbations, adversarial training against l_1 bounded perturbations is shown to be even more time-consuming to achieve the optimal performance (Croce & Hein, 2021). In the case of l_0 bounded perturbations, PGD_0 (Croce & Hein, 2019b) is adopted for adversarial training. However, models trained by PGD_0 exhibit poor robustness against strong sparse attacks. In this work, we propose an effective and efficient sparse attack that enables us to train a model that is more robust against various sparse attacks than existing methods.

4. Methods

In this section, we introduce sparse-PGD (sPGD): a white-box attack that generates sparse perturbations. Similar to AutoAttack (Croce & Hein, 2020; 2021), we further combine sPGD with a black-box attack to construct sparse-AutoAttack (sAA) for more comprehensive and reliable robustness evaluation.

In the end, we incorporate sPGD into the framework of adversarial training to boost the model's robustness against sparse perturbations.

4.1. Sparse-PGD (sPGD)

Inspired by SAIF (Imtiaz et al., 2022), we decompose the sparse perturbation $\boldsymbol{\delta}$ into a magnitude tensor $\boldsymbol{p} \in \mathbb{R}^{h\times w\times c}$ and a sparsity mask $\boldsymbol{m} \in \{0,1\}^{h\times w\times 1}$, i.e., $\boldsymbol{\delta} = \boldsymbol{p}\odot\boldsymbol{m}$. Therefore, the attacker aims to maximize the following loss objective function:

$$\max_{\|\boldsymbol{\delta}\|_0 \le k, 0 \le \boldsymbol{x}+\boldsymbol{\delta} \le 1} \mathcal{L}(\boldsymbol{\theta}, \boldsymbol{x}+\boldsymbol{\delta}) = \max_{\boldsymbol{p}\in\mathcal{S}_{\boldsymbol{p}}, \boldsymbol{m}\in\mathcal{S}_{\boldsymbol{m}}} \mathcal{L}(\boldsymbol{\theta}, \boldsymbol{x}+\boldsymbol{p}\odot\boldsymbol{m}). \tag{3}$$

The feasible sets for $\boldsymbol{p}$ and $\boldsymbol{m}$ are $\mathcal{S}_{\boldsymbol{p}} = \{\boldsymbol{p} \in \mathbb{R}^{h\times w\times c} | 0 \le \boldsymbol{x}+\boldsymbol{p} \le 1\}$ and $\mathcal{S}_{\boldsymbol{m}} = \{\boldsymbol{m} \in \{0,1\}^{h\times w\times 1} | \|\boldsymbol{m}\|_0 \le k\}$, respectively. Similar to PGD, sPGD iteratively updates $\boldsymbol{p}$ and $\boldsymbol{m}$ until finding a successful adversarial example or reaching the maximum iteration number.

Update Magnitude Tensor $\boldsymbol{p}$: The magnitude tensor $\boldsymbol{p}$ is only constrained by the input domain. In the case of images, the input is bounded between 0 and 1. Note that the constraints on $\boldsymbol{p}$ are elementwise and similar to those of l_∞ bounded perturbations. Therefore, instead of greedy or random search (Croce & Hein, 2019b; Croce et al., 2022), we utilize PGD in the l_∞ case, i.e., use the sign of the gradients, to optimize $\boldsymbol{p}$ as demonstrated by Eq. (4) below, with α being the step size.

$$\boldsymbol{p} \longleftarrow \Pi_{\mathcal{S}_{\boldsymbol{p}}} \left(\boldsymbol{p} + \alpha \cdot \mathtt{sign}(\nabla_{\boldsymbol{p}} \mathcal{L}(\boldsymbol{\theta}, \boldsymbol{x} + \boldsymbol{p} \odot \boldsymbol{m}))\right), \quad (4)$$

Update Sparsity Mask $\boldsymbol{m}$: The sparsity mask $\boldsymbol{m}$ is binary and constrained by its l_0 norm. Directly optimizing the discrete variable $\boldsymbol{m}$ is challenging, so we update its continuous alternative $\widetilde{\boldsymbol{m}} \in \mathbb{R}^{h\times w\times 1}$ and project $\widetilde{\boldsymbol{m}}$ to the feasible set $\mathcal{S}_{\boldsymbol{m}}$ to obtain $\boldsymbol{m}$ before multiplying it with the magnitude tensor $\boldsymbol{p}$ to obtain the sparse perturbation $\boldsymbol{\delta}$. Specifically, $\widetilde{\boldsymbol{m}}$ is updated by gradient ascent. Projecting $\widetilde{\boldsymbol{m}}$ to the feasible set $\mathcal{S}_{\boldsymbol{m}}$ is to set the k-largest elements in $\widetilde{\boldsymbol{m}}$ to 1 and the rest to 0. In addition, we adopt the sigmoid function to normalize the elements of $\widetilde{\boldsymbol{m}}$ before projection.

Mathematically, the update rules for $\widetilde{\boldsymbol{m}}$ and $\boldsymbol{m}$ are demonstrated as follows:

$$\widetilde{\boldsymbol{m}} \longleftarrow \widetilde{\boldsymbol{m}} + \beta \cdot \nabla_{\widetilde{\boldsymbol{m}}} \mathcal{L} / ||\nabla_{\widetilde{\boldsymbol{m}}} \mathcal{L}||_2, \quad (5)$$

$$\boldsymbol{m} \longleftarrow \Pi_{\mathcal{S}_{\boldsymbol{m}}}(\sigma(\widetilde{\boldsymbol{m}})) \quad (6)$$

where β is the step size for updating the sparsity mask's continuous alternative $\widetilde{\boldsymbol{m}}$, $\sigma(\cdot)$ denotes the sigmoid function. Furthermore, to prevent the magnitude of $\widetilde{\boldsymbol{m}}$ from becoming explosively large, we do not update $\widetilde{\boldsymbol{m}}$ when $||\nabla_{\widetilde{\boldsymbol{m}}} \mathcal{L}||_2 < \gamma$, which indicates that $\widetilde{\boldsymbol{m}}$ is located in the saturation zone of sigmoid function. The gradient $\nabla_{\widetilde{\boldsymbol{m}}} \mathcal{L}$ is calculated at the point $\boldsymbol{\delta} = \boldsymbol{p} \odot \Pi_{\mathcal{S}_{\boldsymbol{m}}}(\sigma(\widetilde{\boldsymbol{m}}))$, where the loss function is not always differentiable. We demonstrate how to estimate the update direction in the next part.

Backward Function: Based on Eq. (3), we can calculate the gradient of the magnitude tensor $\boldsymbol{p}$ by $\nabla_{\boldsymbol{p}} \mathcal{L} = \nabla_{\boldsymbol{\delta}} \mathcal{L}(\boldsymbol{\theta}, \boldsymbol{x} + \boldsymbol{\delta}) \odot \boldsymbol{m}$ and use $g_{\boldsymbol{p}}$ to represent this gradient for notation simplicity. At most, k non-zero elements are in the mask $\boldsymbol{m}$, so $g_{\boldsymbol{p}}$ is sparse and has at most k non-zero elements. That is to say, we update at most k elements of the magnitude tensor $\boldsymbol{p}$ based on the gradient $g_{\boldsymbol{p}}$. Like coordinate descent, this may result in suboptimal performance since most elements of $\boldsymbol{p}$ are unchanged in each iterative update. To tackle this problem, we discard the projection to the binary set $\mathcal{S}_{\boldsymbol{m}}$ when calculating the gradient and use the *unprojected gradient* $\widetilde{g}_{\boldsymbol{p}}$ to update $\boldsymbol{p}$. Based on Eq. (6), we have $\widetilde{g}_{\boldsymbol{p}} = \nabla_{\boldsymbol{\delta}} \mathcal{L}(\boldsymbol{\theta}, \boldsymbol{x} + \boldsymbol{\delta}) \odot \sigma(\widetilde{\boldsymbol{m}})$. The idea of the unprojected gradient is inspired by training pruned neural networks and lottery ticket hypothesis (Frankle & Carbin, 2019; Ramanujan et al., 2020; Fu et al., 2021; Liu et al., 2022). All these methods train importance scores to prune the model parameters but update the importance scores based on the whole network instead of the pruned sub-network to prevent the sparse update, which leads to suboptimal performance.

Algorithm 1 Sparse-PGD

```
Input: Clean image: $\boldsymbol{x} \in [0,1]^{h\times w\times c}$; Model parameters: $\boldsymbol{\theta}$; Max iteration number: $T$; Tolerance: $t$; $l_0$ budget: $k$; Step size: $\alpha$, $\beta$; Small constant: $\gamma = 2 \times 10^{-8}$
Random initialize $\boldsymbol{p}$ and $\widetilde{\boldsymbol{m}}$
for $i = 0, 1, ..., T-1$ do
    $\boldsymbol{m} = \Pi_{\mathcal{S}_{\boldsymbol{m}}}(\sigma(\widetilde{\boldsymbol{m}}))$
    Calculate the loss $\mathcal{L}(\boldsymbol{\theta}, \boldsymbol{x} + \boldsymbol{p} \odot \boldsymbol{m})$
    if unprojected then
        $g_{\boldsymbol{p}} = \nabla_{\boldsymbol{\delta}} \mathcal{L} \odot \sigma(\widetilde{\boldsymbol{m}})$        $\{\boldsymbol{\delta} = \boldsymbol{p} \odot \boldsymbol{m}\}$
    else
        $g_{\boldsymbol{p}} = \nabla_{\boldsymbol{\delta}} \mathcal{L} \odot \boldsymbol{m}$
    end if
    $g_{\widetilde{\boldsymbol{m}}} = \nabla_{\boldsymbol{\delta}} \mathcal{L} \odot \boldsymbol{p} \odot \sigma'(\widetilde{\boldsymbol{m}})$
    $\boldsymbol{p} = \Pi_{\mathcal{S}_{\boldsymbol{p}}}(\boldsymbol{p} + \alpha \cdot \mathtt{sign}(g_{\boldsymbol{p}}))$
    $\boldsymbol{d} = g_{\widetilde{\boldsymbol{m}}} / (||g_{\widetilde{\boldsymbol{m}}}||_2)$ if $||g_{\widetilde{\boldsymbol{m}}}||_2 \geq \gamma$ else $0$
    $\boldsymbol{m}_{old}$, $\widetilde{\boldsymbol{m}} = \boldsymbol{m}$, $\widetilde{\boldsymbol{m}} + \beta \cdot \boldsymbol{d}$
    if attack succeeds then
        break
    end if
    if $||\Pi_{\mathcal{S}_{\boldsymbol{m}}}(\sigma(\widetilde{\boldsymbol{m}})) - \boldsymbol{m}_{old}||_0 \leq 0$ for $t$ consecutive iters then
        Random initialize $\widetilde{\boldsymbol{m}}$
    end if
end for
Output: Perturbation: $\boldsymbol{\delta} = \boldsymbol{p} \odot \boldsymbol{m}$
```

In practice, the performance of using $g_{\boldsymbol{p}}$ and $\widetilde{g}_{\boldsymbol{p}}$ to optimize $\boldsymbol{p}$ is complementary. The sparse gradient $g_{\boldsymbol{p}}$ is consistent with the forward propagation and is thus better at exploitation. By contrast, the unprojected gradient $\widetilde{g}_{\boldsymbol{p}}$ updates the $\boldsymbol{p}$ by a dense tensor and is thus better at exploration. In view of this, we set up an ensemble of attacks with both gradients to balance exploration and exploitation.

When calculating the gradient of the continuous alternative $\widetilde{\boldsymbol{m}}$, we have $\frac{\partial \mathcal{L}}{\partial \widetilde{\boldsymbol{m}}} = \frac{\partial \mathcal{L}(\boldsymbol{\theta}, \boldsymbol{x} + \boldsymbol{\delta})}{\partial \boldsymbol{\delta}} \odot \boldsymbol{p} \odot \frac{\partial \Pi_{\mathcal{S}_{\boldsymbol{m}}}(\sigma(\widetilde{\boldsymbol{m}}))}{\partial \widetilde{\boldsymbol{m}}}$. Since the projection to the set $\mathcal{S}_{\boldsymbol{m}}$ is not always differentiable, we discard the projection operator and use the approximation $\frac{\partial \Pi_{\mathcal{S}_{\boldsymbol{m}}}(\sigma(\widetilde{\boldsymbol{m}}))}{\partial \widetilde{\boldsymbol{m}}} \simeq \sigma'(\widetilde{\boldsymbol{m}})$ to calculate the gradient.

Random Reinitialization: Due to the projection to the set $\mathcal{S}_{\boldsymbol{m}}$ in Eq. (6), the sparsity mask $\boldsymbol{m}$ changes only when the relative magnitude ordering of the continuous alternative $\widetilde{\boldsymbol{m}}$ changes. In other words, slight changes in $\widetilde{\boldsymbol{m}}$ usually mean no change in $\boldsymbol{m}$. As a result, $\boldsymbol{m}$ usually gets trapped in a local maximum. To solve this problem, we propose a random reinitialization mechanism. Specifically, when the attack fails, i.e., the model still gives the correct prediction, and the current sparsity mask $\boldsymbol{m}$ remains unchanged for three consecutive iterations, the continuous alternative $\widetilde{\boldsymbol{m}}$ will be randomly reinitialized for better exploration.

To summarize, we provide the pseudo-code of sparse PGD (sPGD) in Algorithm 1. SAIF (Imtiaz et al., 2022) also decomposes the perturbation $\boldsymbol{\delta}$ into a magnitude tensor $\boldsymbol{p}$ and a mask $\boldsymbol{m}$, but uses a different update rule: it uses Frank-Wolfe to update both $\boldsymbol{p}$ and $\boldsymbol{m}$. By contrast, we introduce the continuous alternative $\widetilde{\boldsymbol{m}}$ of $\boldsymbol{m}$ and use gradient ascent to update $\boldsymbol{p}$ and $\widetilde{\boldsymbol{m}}$. Moreover, we include unprojected gradient and random reinitialization techniques in Algorithm 1 to further enhance the performance.

4.2. Sparse-AutoAttack (sAA)

AutoAttack (AA) (Croce & Hein, 2020) is an ensemble of four diverse attacks for a standardized parameters-free and reliable evaluation of robustness against l_∞ and l_2 attacks. Croce & Hein (2021) extends AutoAttack to l_1 bounded perturbations. In this work, we propose sparse-AutoAttack (sAA), which is also a parameter-free ensemble of both black-box and white-box attacks for comprehensive robustness evaluation against l_0 bounded perturbations. It can be used in a plug-and-play manner. However, different from the l_∞, l_2 and l_1 cases, the adaptive step size, momentum and difference of logits ratio (DLR) loss function do not improve the performance in the l_0 case, so they are not adopted in sAA. In addition, compared with targeted attacks, sPGD turns out stronger when using a larger query budget in the untargeted settings given the same total number of back-propagations. As a result, we only include the untargeted sPGD with cross-entropy loss and constant step sizes in sAA. Specifically, we run sPGD twice for two different backward functions: one denoted as sPGD$_{\mathrm{proj}}$ uses the sparse gradient $g_{\boldsymbol{p}}$, and the other denoted as sPGD$_{\mathrm{unproj}}$ uses the unprojected gradient $\widetilde{g}_{\boldsymbol{p}}$ as described in Section 4.1. As for the black-box attack, we adopt the strong black-box attack Sparse-RS (Croce et al., 2022), which can generate l_0 bounded perturbations. We run each version of sPGD and Sparse-RS for 10000 iterations, respectively. We use cascade evaluation to improve the efficiency. Concretely, suppose we find a successful adversarial perturbation by one attack for one instance. Then, we will consider the model non-robust in this instance and the same instance will not be further evaluated by other attacks. Based on the efficiency and the attack success rate, the attacks in sAA are sorted in the order of **sPGD**$_{\mathrm{unproj}}$, **sPGD**$_{\mathrm{proj}}$ and **Sparse-RS**.

4.3. Adversarial Training

In addition to robustness evaluation, we also explore adversarial training to build robust models against sparse perturbations. In the framework of adversarial training, the attack is used to generate adversarial perturbation in each training iteration, so the attack algorithm should not be too computationally expensive. In this regard, we run the untargeted sPGD (Algorithm 1) for 20 iterations to generate sparse adversarial perturbations during training. We incorporate sPGD in the framework of vanilla adversarial training (Madry et al., 2017) and TRADES (Zhang et al., 2019b) and name corresponding methods **sAT** and **sTRADES**, respectively. Note that we use sAT and sTRADES as two examples of applying sPGD to adversarial training, since sPGD can be incorporated into any other adversarial training variant as well. To accommodate the scenario of adversarial training, we make the following modifications to sPGD.

Random Backward Function: Since the sparse gradient and the unprojected gradient as described in Section 4.1 induce different exploration-exploitation trade-offs, we randomly select one of them to generate adversarial perturbations for each mini-batch when using sPGD to generate adversarial perturbations. Compared with mixing these two backward functions together, as in sAA, random backward function does not introduce computational overhead.

Multi-k Strategy: Inspired by l_1-APGD (Croce & Hein, 2021) and Fast-EG-l_1 (Jiang et al., 2023), multi-k strategy is adopted to strengthen the robustness of model. That is, we use a larger sparsity threshold, i.e., k in Algorithm 1, in the training phase than in the test phase.

Higher Tolerance for Reinitialization: The default tolerance for reinitialization in sPGD is 3 iterations, which introduces strong stochasticity. However, in the realm of adversarial training, we have a limited number of iterations. As a result, the attacker should focus more on the exploitation ability to ensure the strength of the generated adversarial perturbations. While stochasticity introduced by frequent reinitialization hurts exploitation, we find a higher tolerance for reinitialization improves the performance. In practice, we set the tolerance to 10 iterations in adversarial training.

5. Experiments

In this section, we conduct extensive experiments to compare our attack methods with baselines in evaluating the robustness of various models against l_0 bounded perturbations. Besides the effectiveness with an abundant query budget, we also study the efficiency of our methods when using limited iterations to generate adversarial perturbations. Our results demonstrate that our sPGD performs best among white-box attacks. With limited iterations, sPGD achieves significantly better performance than existing methods. Therefore, sAA, consisting of the best white-box and black-box attacks, has the best attack success rate. sPGD, due to its efficiency, is utilized for adversarial training to obtain the best robust models against l_0 bounded adversarial perturbations. To further demonstrate the efficiency and efficacy of our method, we compare the runtime of different attacks and evaluate the transferability of sPGD. The results show that sPGD has a high transfer success rate, making it applicable in more practical scenarios. In addition, we conduct ablation studies for analysis. The adversarial examples generated by our methods are presented in Appendix C. Implementation details are deferred to Appendix B.

5.1. Evaluation of Different Attack Methods

First, we compare our proposed sPGD, including $\text{sPGD}_{\text{proj}}$ and $\text{sPGD}_{\text{unproj}}$ as defined in Section 4.2, and sAA with existing white-box and black-box attacks that generate sparse perturbations. We evaluate different attack methods based on the models trained on CIFAR-10 (Krizhevsky et al., 2009) and report the robust accuracy with $k = 20$ on the whole test set in Table 1. Additionally, the results on ImageNet100 (Deng et al., 2009) and a real-world traffic sign dataset GTSRB (Stallkamp et al., 2012) are reported in Table 2. Note that the image sizes in GTSRB vary from 15×15 to 250×250. For convenience, we resize them to 224×224 and use the same model architecture as in ImageNet-100. Furthermore, only the training set of GTSRB has annotations, we manually split the original training set into a test set containing 1000 instances and a new training set containing the rest data. In Appendix A.1, we report more results on CIFAR-10 with $k = 10$, $k = 15$, and the results of models trained on CIFAR-100 (Krizhevsky et al., 2009) in Table 8, 9, 10, respectively to comprehensively demonstrate the effectiveness of our methods.

Models: We select various models to comprehensively evaluate their robustness against l_0 bounded perturbations. As a baseline, we train a ResNet-18 (RN-18) (He et al., 2016a) model on clean inputs. For adversarially trained models, we select competitive models that are publicly available, including those trained against l_∞, l_2 and l_1 bounded perturbations. For the l_∞ case, we include adversarial training with the generated data (GD) (Gowal et al., 2021), the proxy distributions (PORT) (Sehwag et al., 2021), the decoupled KL divergence loss (DKL) (Cui et al., 2023) and strong diffusion models (DM) (Wang et al., 2023). For the l_2 case, we include adversarial training with the proxy distributions (PORT) (Sehwag et al., 2021), strong diffusion models (DM) (Wang et al., 2023), helper examples (HAT) (Rade & Moosavi-Dezfooli, 2021) and strong data augmentations (FDA) (Rebuffi et al., 2021). The l_1 case is less explored in the literature, so we only include l_1-APGD adversarial training (Croce & Hein, 2021) and the efficient Fast-EG-l_1 (Jiang et al., 2023) for comparison. The network architecture used in these baselines is either ResNet-18 (RN-18), PreActResNet-18 (PRN-18) (He et al., 2016b) or WideResNet-28-10 (WRN-28) (Zagoruyko & Komodakis, 2016). For the l_0 case, we evaluate PGD_0 (Croce & Hein, 2019b) in vanilla adversarial training (PGD_0-A) and TRADES (PGD_0-T) using the same hyper-parameter settings as in Croce & Hein (2019b). Since other white-box sparse attacks present trivial performance in adversarial training, we do not include their results. Finally, we use our proposed sPGD in vanilla adversarial training (sAT) and TRADES (sTRADES) to obtain PRN-18 models to compare with these baselines.

Attacks: We compare our methods with various existing black-box and white-box attacks that generate l_0 bounded perturbations. The black-box attacks include CornerSearch (CS) (Croce & Hein, 2019b) and Sparse-RS (RS) (Croce et al., 2022). The white-box attacks include SparseFool (SF) (Modas et al., 2018), PGD_0 (Croce & Hein, 2019b) and Sparse Adversarial and Interpretable Attack Framework (SAIF) (Imtiaz et al., 2022). The implementation details of each attack are deferred to Appendix B. Specifically, to exploit the strength of these attacks in reasonable running time, we run all these attacks for either 10000 iterations or the number of iterations where their performances converge. Note that, the number of iterations for all these attacks are no smaller than their default settings. In addition, we report the results of RS with fine-tuned hyperparameters, which outperforms its default settings in (Croce et al., 2022). Finally, we report the robust accuracy under CS attack based on only 1000 random test instances due to its prohibitively high computational complexity.

Based on the results in Table 1 and Table 2, we can find that SF attack, PGD_0 attack and SAIF attack perform significantly worse than our methods for all the models studied. That is, our proposed sPGD always performs the best among white-box attacks. Among black-box attacks, CS attack can achieve competitive performance, but it runs dozens of times longer than our method does. Therefore, we focus on comparing our method with RS attack. For l_1 and l_2 models, our proposed sPGD significantly outperforms RS attack. By contrast, RS attack outperforms sPGD for l_∞ and l_0 models. This gradient masking phenomenon is, in fact, prevalent across sparse attacks. Given sufficient iterations, RS outperforms all other existing white-box attacks for l_∞ and l_0 models. Nevertheless, among white-box attacks, sPGD exhibits the least susceptibility to gradient masking and has the best performance. The occurrence of gradient masking in the context of l_0 bounded perturbations can be attributed to the non-convex nature of adversarial budgets. In practice, the perturbation updates often significantly deviate from the direction of the gradients because of the projection to the non-convex set. Similar to AA in the l_1, l_2 and l_∞ cases, sAA consists of both white-box and black-box attacks for comprehensive robustness evaluation. It achieves the best performance in all cases in Table 1 and Table 2 by a considerable margin.

In the case of l_0 adversarial training, the models are adversarially trained against sparse attacks. However, Figure 1 illustrates that the performance of RS attack drastically deteriorates with limited iterations (e.g., smaller than 100), so RS is not suitable for adversarial training where we need to generate strong adversarial perturbations in limited num-

Table 1. Robust accuracy of various models on different attacks that generate l_0 bounded perturbations, where the sparsity level $k = 20$. The models are trained on **CIFAR-10**. Note that we report results of Sparse-RS (RS) with fine-tuned hyperparameters, which outperforms its original version in Croce et al. (2022). CornerSearch (CS) is evaluated on 1000 samples due to its high computational complexity.

Model	Network	Clean	Black-Box		White-Box					sAA
			CS	RS	SF	PGD_0	SAIF	$\textbf{sPGD}_{\text{proj}}$	$\textbf{sPGD}_{\text{unproj}}$	
Vanilla	RN-18	93.9	1.2	0.0	17.5	0.4	3.2	0.0	0.0	**0.0**
l_∞-adv. trained, $\epsilon = 8/255$										
GD	PRN-18	87.4	26.7	6.1	52.6	25.2	40.4	9.0	15.6	**5.3**
PORT	RN-18	84.6	27.8	8.5	54.5	21.4	42.7	9.1	14.6	**6.7**
DKL	WRN-28	92.2	33.1	7.0	54.0	29.3	41.1	9.9	15.8	**6.1**
DM	WRN-28	92.4	32.6	6.7	49.4	26.9	38.5	9.9	15.1	**5.9**
l_2-adv. trained, $\epsilon = 0.5$										
HAT	PRN-18	90.6	34.5	12.7	56.3	22.5	49.5	9.1	8.5	**7.2**
PORT	RN-18	89.8	30.4	10.5	55.0	17.2	48.0	6.3	5.8	**4.9**
DM	WRN-28	95.2	43.3	14.9	59.2	31.8	59.6	13.5	12.0	**10.2**
FDA	WRN-28	91.8	43.8	18.8	64.2	25.5	57.3	15.8	19.2	**14.1**
l_1-adv. trained, $\epsilon = 12$										
l_1-APGD	PRN-18	80.7	32.3	25.0	65.4	39.8	55.6	17.9	18.8	**16.9**
Fast-EG-l_1	PRN-18	76.2	35.0	24.6	60.8	37.1	50.0	18.1	18.6	**16.8**
l_0-adv. trained, $k = 20$										
PGD_0-A	PRN-18	77.5	16.5	2.9	62.8	56.0	47.9	9.9	21.6	**2.4**
PGD_0-T	PRN-18	90.0	24.1	4.9	85.1	61.1	67.9	27.3	37.9	**4.5**
sAT	PRN-18	84.5	52.1	36.2	81.2	78.0	76.6	75.9	75.3	**36.2**
sTRADES	PRN-18	89.8	69.9	61.8	88.3	86.1	84.9	84.6	81.7	**61.7**

Table 2. Robust accuracy of various models on different attacks that generate l_0 bounded perturbations. ResNet34 (RN-34) (He et al., 2016a) is used as the network architecture. Our sAT model is trained with the sparsity level $k = 1200$ and the iteration number of the attack $t = 20$. **(a)** The models are trained on **ImageNet-100** (Deng et al., 2009), and the k for attacks is set to 200. **(b)** The models are trained on **GTSRB** (Stallkamp et al., 2012), and the k for attacks is set to 600. Note that we report results of Sparse-RS (RS) with tuned hyperparameters, which outperforms its original version in Croce et al. (2022). All methods are evaluated on 500 samples, and CornerSearch (CS) is not evaluated here due to its high computational complexity, i.e. nearly 1 week on one GPU for each run.

(a) **ImageNet,** $k = 200$

Model	Network	Clean	Black-Box		White-Box					sAA
			CS	RS	SF	PGD_0	SAIF	$\textbf{sPGD}_{\text{proj}}$	$\textbf{sPGD}_{\text{unproj}}$	
Vanilla	RN-34	83.0	-	0.2	5.8	9.8	0.6	0.2	0.4	**0.0**
l_1-adv. trained, $\epsilon = 72$										
Fast-EG-l_1	RN-34	69.2	-	50.2	43.4	50.2	43.0	18.6	19.0	**16.6**
l_0-adv. trained, $k = 200$										
PGD_0-A	RN-34	76.0	-	6.8	57.2	37.4	11.0	1.8	18.8	**1.8**
sAT	RN-34	86.2	-	61.4	84.2	83.0	69.0	78.0	77.8	**61.2**

(b) **GTSRB,** $k = 600$

Model	Network	Clean	Black-Box		White-Box					sAA
			CS	RS	SF	PGD_0	SAIF	$\textbf{sPGD}_{\text{proj}}$	$\textbf{sPGD}_{\text{unproj}}$	
Vanilla	RN-34	99.9	-	18.0	18.9	63.7	9.5	**0.3**	**0.3**	**0.3**
l_0-adv. trained, $k = 600$										
PGD_0-A	RN-34	99.8	-	37.6	23.6	59.8	13.8	**0.0**	**0.0**	**0.0**
sAT	RN-34	99.8	-	88.4	96.8	99.8	96.2	88.6	96.2	**85.4**

ber iterations. Empirical evidence suggests that employing RS with 20 iterations for adversarial training, i.e., the same number of iterations as in other methods, yields trivial performance, so it is not included in Table 1 or Table 2 for comparison. In addition, models trained by PGD_0-A and PGD_0-T, which generate l_0 bounded perturbations, exhibit

Table 3. Runtime of different attacks on 1000 test instances with batch size 500. The sparsity level $k = 20$. The evaluated model is sTRADES. The model is trained on **CIFAR-10**. The experiments are implemented on NVIDIA Tesla V100.

Attack	CS	RS	SF	PGD$_0$	SAIF	**sPGD**$_{\text{proj}}$	**sPGD**$_{\text{unproj}}$	**sAA**
Runtime	604 min	59 min	92 min	750 min	122 min	**42 min**	45 min	148 min

poor robustness to various attack methods, especially sAA. By contrast, the models trained by sAT and sTRADES show the strongest robustness, indicated by the comprehensive sAA method and all other attack methods. Compared with sAT, sTRADES achieves better performance in both robustness and accuracy. Finally, models trained with l_1 bounded perturbations are the most robust ones among existing non-l_0 training methods. It could be attributed to the fact that l_1 norm is the tightest convex relaxation of l_0 norm (Bittar et al., 2021). From a qualitative perspective, l_1 attacks also generate relatively sparse perturbations (Jiang et al., 2023), which makes the corresponding model robust to sparse perturbations to some degree.

Our results indicate sPGD and RS can complement each other. Therefore, sAA, an AutoAttack-style attack that ensembles both attacks achieves the state-of-the-art performance on all models. It is designed to have a similar computational complexity to AutoAttack in l_∞, l_2 and l_1 cases.

5.2. Comparison under Different Iteration Numbers

In this subsection, we further compare our method sPGD, which is a white-box attack, with RS attack, the strongest black-box attack in the previous section. Specifically, we compare them under various iteration numbers on CIFAR-10 and ImageNet-100, which have different resolutions. Since CIFAR-100 has the same resolution as CIFAR-10, the results on CIFAR-100 are deferred to Appendix A.2. In addition, we also compare sPGD and RS under different sparsity levels in Appendix A.3.

As illustrated in Figure 1, sTRADES has better performance than other robust models by a large margin in all iterations of both sPGD and RS attacks, which is consistent with the results in Table 1, 2 and 10. For vanilla and other robust models, although the performances of both sPGD and RS attack get improved with more iterations, sPGD outperforms RS attack by a large margin when the iteration number is small (e.g. < 1000 iterations), which makes it feasible for adversarial training. Similar to other black-box attacks, the performance of RS attack drastically deteriorates when the query budget is limited. In addition, our proposed gradient-based sPGD significantly outperforms RS on ImageNet-100, where the search space is much larger than that on CIFAR-10, i.e., higher image resolution and higher sparsity level k. This suggests that our approach is scalable and shows higher efficiency on high-resolution images. Furthermore, although the performance of RS does not converge even when the iteration number reaches 10000, a larger query budget will make it computationally impractical. Following the setting in Croce et al. (2022), we do not consider a larger query budget in our experiments, either. To further showcase the efficiency of our approach, we compare the distributions of the number of iterations needed by sPGD and RS to successfully generate adversarial samples Appendix A.4.

5.3. Runtime of Different Attacks

As shown in Table 3, the proposed sPGD shows the highest efficiency among various attacks. Although sAA consumes more time (approximately 2× sPGD + RS), it can provide a reliable evaluation against l_0 bounded perturbation.

5.4. Transferability of Adversarial Perturbations

Table 4. Transferability of RS and sPGD between VGG11 (V) and ResNet18 (R). The results are reported in attack success rate (ASR). The perturbation is generated based on the source model (left), and the ASR is obtained on the target model (right). The evaluated dataset is CIFAR-10 (Krizhevsky et al., 2009), and the sparsity level $k = 20$. Note that the models are trained on clean instances, and the step-size of sPGD α and β are set to 0.75.

Attack	V→V	V→R	R→R	R→V
RS	53.9	28.4	33.0	37.4
sPGD$_{\text{proj}}$	58.0	**43.9**	50.8	48.0
sPGD$_{\text{unproj}}$	**64.9**	40.0	**52.7**	**56.7**

To evaluate the transferability of our attack across different models and architectures, we generate adversarial perturbations based on one model and report the attack success rate (ASR) on another model. As shown in Table 4, sPGD exhibits better transferability than the most competitive baseline, Sparse-RS (RS) (Croce et al., 2022). This further demonstrates the effectiveness of our method and its potential application in more practical scenarios.

5.5. Ablation Studies

We conduct ablation studies in this section. We focus on CIFAR10 and the sparsity level $k = 20$. Unless specified, we use the same configurations as in Table 1.

Components of sPGD: We first validate the effectiveness of each component in sPGD. The result is reported in Table 5. We observe that naively decomposing the perturbation $\boldsymbol{\delta}$ by $\boldsymbol{\delta} = \boldsymbol{p} \odot \boldsymbol{m}$ and updating them separately can deteriorate the performance. By contrast, the performance significantly improves when we update the mask $\boldsymbol{m}$ by its continuous alternative $\widetilde{\boldsymbol{m}}$ and l_0 ball projection. This indicates that in-

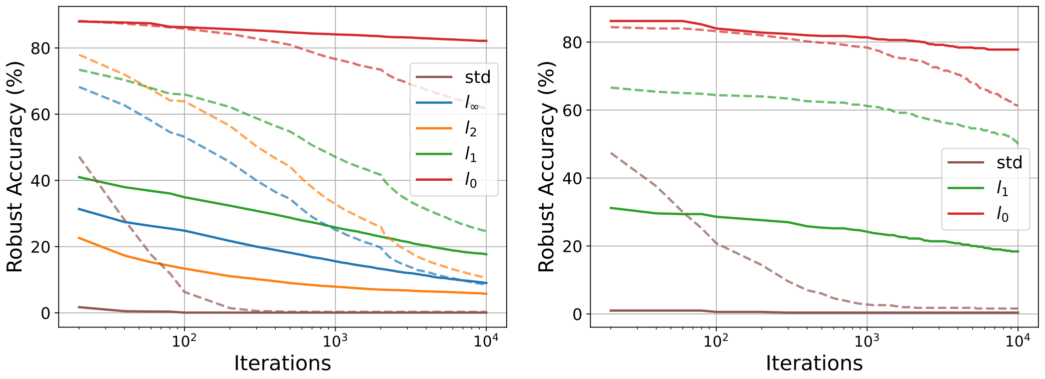

(a) CIFAR-10, $k = 20$ (b) ImageNet-100, $k = 200$

Figure 1. Comparison between sPGD and RS attack under different iterations. **(a)** CIFAR-10, $k = 20$. ResNet18 (std), PORT (l_∞ and l_2) (Sehwag et al., 2021), l_1-APGD (l_1) (Croce & Hein, 2021) and sTRADES (l_0) are evaluated. **(b)** ImageNet-100, $k = 200$. ResNet34 (std), Fast-EG-l_1 (l_1) (Jiang et al., 2023) and sAT (l_0) are evaluated. The total iteration number ranges from 20 and 10000. **The results of sPGD and RS attack are shown in solid lines and dotted lines, respectively.** For better visualization, the x-axis is in the log scale.

troducing $\widetilde{\boldsymbol{m}}$ greatly mitigates the challenges in optimizing discrete variables. Moreover, the results in Table 5 indicate the performance can be further improved by the random reinitialization mechanism, which encourages exploration and avoids trapping in a local optimum. In Appendix A.5, we compare the performance when we use different step sizes for the magnitude tensor $\boldsymbol{p}$ and the sparsity mask $\boldsymbol{m}$. The results in Table 11 and 12 of Appendix A.5 indicate that the performance of our proposed method is quite consistent under different choices of step sizes, which facilities hyper-parameter selection for practitioners.

Table 5. Ablation study of each component in sPGD$_{\text{proj}}$ in terms of robust accuracy. The model is trained by Fast-EG-l_1.

Ablations	Robust Acc.
Baseline (PGD$_0$ w/o restart)	49.4
+ Decomposition: $\boldsymbol{\delta} = \boldsymbol{p} \odot \boldsymbol{m}$	58.0 (+8.6)
+ Continuous mask $\widetilde{\boldsymbol{m}}$	33.9 (-15.5)
+ Random reinitialization	**18.1 (-31.3)**

Adversarial training: We conduct preliminary exploration on adversarial training against sparse perturbations, since sPGD can be incorporated into any adversarial training variant. Table 1, 2, 8, 9 and 10 study sAT and sTRADES, while sTRADES outperforms sAT in all cases. In addition, the training of sAT is relatively unstable in practice, so we focus on sTRADES for ablation studies in this section. We leave the design of sPGD-adapted adversarial training variants to further improve model robustness as a future work.

Table 6 demonstrates the performance when we use different backward functions. The policies include always using the sparse gradient (Proj.), always using the unprojected gradient (Unproj.), alternatively using both backward functions every 5 epochs (Alter.) and randomly selecting backward functions (Rand.). The results indicate that randomly selecting backward functions has the best performance. In addition, Table 7 demonstrates the robust accuracy of models trained by sTRADES with different multi-k strategies. The results indicate that multi-k strategy helps boost the performance. The best robust accuracy is obtained when the adversarial budget for training is 6 times larger than that for test. Furthermore, we also study the impact of different tolerances during adversarial training in Table 14 of Appendix A.6. The results show that higher tolerance during adversarial training benefits the robustness of the model.

Table 6. Ablation study on different policies during adversarial training. The model is PRN18 trained by sTRADES with $6 \times k$. The robust accuracy is obtained through sAA.

Policy	Proj.	Unproj.	Alter.	Rand.
Acc.	41.5	39.4	51.5	**61.7**

Table 7. Ablation study on multi-k stretegy during adversarial training. The model is PRN18 trained by sTRADES with random policy. The robust accuracy is obtained through sAA.

k	1×	2×	4×	6×	8×	10×
Acc.	34.0	39.7	54.5	**61.7**	60.2	55.5

6. Conclusion

In this paper, we propose an effective and efficient white-box attack named sPGD to generate perturbations bounded by l_0 norm. sPGD obtains the state-of-the-art performance among white-box attacks. Based on this, we combine it with black-box attacks for more comprehensive and reliable l_0 robustness evaluation. Our proposed sPGD is particularly effective in the realm of limited iteration numbers. Due to its efficiency, we incorporate sPGD into the framework of adversarial training to obtain robust models against sparse perturbations. The models trained with our method demonstrate the best robust accuracy.

Impact Statement

We adopt 20-iter sPGD in adversarial training, so the computational overhead is still high, making it difficult to scale up to super-large datasets. Our subsequent work will focus on developing a faster adversarial training method against l_0 bounded perturbations without sacrificing its robustness. Furthermore, since our method is evaluated on benchmarks, we do not see it has an obvious negative societal impact.

Acknowledgement

This work is supported by National Natural Science Foundation of China (NSFC Project No. 62306250), CityU APRC Project (Project No. 9610614), and CityU Seed Grant (Project No. 9229130).

References

Akhtar, N. and Mian, A. S. Threat of adversarial attacks on deep learning in computer vision: A survey. *IEEE Access*, 6:14410–14430, 2018. URL `https://api.semanticscholar.org/CorpusID:3536399`.

Al-Dujaili, A. and O'Reilly, U.-M. There are no bit parts for sign bits in black-box attacks. *ArXiv*, abs/1902.06894, 2019. URL `https://api.semanticscholar.org/CorpusID:67749599`.

Alzantot, M. F., Sharma, Y., Chakraborty, S., and Srivastava, M. B. Genattack: practical black-box attacks with gradient-free optimization. *Proceedings of the Genetic and Evolutionary Computation Conference*, 2018. URL `https://api.semanticscholar.org/CorpusID:44166696`.

Andriushchenko, M. and Flammarion, N. Understanding and improving fast adversarial training. *ArXiv*, abs/2007.02617, 2020. URL `https://api.semanticscholar.org/CorpusID:220363591`.

Andriushchenko, M., Croce, F., Flammarion, N., and Hein, M. Square attack: a query-efficient black-box adversarial attack via random search. *ArXiv*, abs/1912.00049, 2019. URL `https://api.semanticscholar.org/CorpusID:208527215`.

Athalye, A., Carlini, N., and Wagner, D. A. Obfuscated gradients give a false sense of security: Circumventing defenses to adversarial examples. In *International Conference on Machine Learning*, 2018. URL `https://api.semanticscholar.org/CorpusID:3310672`.

Bhagoji, A. N., He, W., Li, B., and Song, D. X. Practical black-box attacks on deep neural networks using efficient query mechanisms. In *European Conference on Computer Vision*, 2018. URL `https://api.semanticscholar.org/CorpusID:52951839`.

Bittar, T., Chancelier, J.-P., and Lara, M. D. Best convex lower approximations of the l 0 pseudonorm on unit balls. 2021. URL `https://api.semanticscholar.org/CorpusID:235254019`.

Carlini, N. and Wagner, D. Towards evaluating the robustness of neural networks. In *2017 ieee symposium on security and privacy (sp)*, pp. 39–57. Ieee, 2017.

Croce, F. and Hein, M. Minimally distorted adversarial examples with a fast adaptive boundary attack. *ArXiv*, abs/1907.02044, 2019a. URL `https://api.semanticscholar.org/CorpusID:195791557`.

Croce, F. and Hein, M. Sparse and imperceivable adversarial attacks. In *Proceedings of the IEEE/CVF international conference on computer vision*, pp. 4724–4732, 2019b.

Croce, F. and Hein, M. Reliable evaluation of adversarial robustness with an ensemble of diverse parameter-free attacks. In *International conference on machine learning*, pp. 2206–2216. PMLR, 2020.

Croce, F. and Hein, M. Mind the box: *l*_1-apgd for sparse adversarial attacks on image classifiers. In *International Conference on Machine Learning*, pp. 2201–2211. PMLR, 2021.

Croce, F., Andriushchenko, M., Sehwag, V., Debenedetti, E., Flammarion, N., Chiang, M., Mittal, P., and Hein, M. Robustbench: a standardized adversarial robustness benchmark. *arXiv preprint arXiv:2010.09670*, 2020.

Croce, F., Andriushchenko, M., Singh, N. D., Flammarion, N., and Hein, M. Sparse-rs: a versatile framework for query-efficient sparse black-box adversarial attacks. In *Proceedings of the AAAI Conference on Artificial Intelligence*, volume 36, pp. 6437–6445, 2022.

Cui, J., Tian, Z., Zhong, Z., Qi, X., Yu, B., and Zhang, H. Decoupled kullback-leibler divergence loss. *ArXiv*, abs/2305.13948, 2023. URL `https://api.semanticscholar.org/CorpusID:258841423`.

de Jorge, P., Bibi, A., Volpi, R., Sanyal, A., Torr, P. H. S., Rogez, G., and Dokania, P. K. Make some noise: Reliable and efficient single-step adversarial training. *ArXiv*, abs/2202.01181, 2022. URL `https://api.semanticscholar.org/CorpusID:246473010`.

Deng, J., Dong, W., Socher, R., Li, L.-J., Li, K., and Fei-Fei, L. ImageNet: A Large-Scale Hierarchical Image Database. In *CVPR09*, 2009.

Dong, X., Chen, D., Bao, J., Qin, C., Yuan, L., Zhang, W., Yu, N., and Chen, D. Greedyfool: Distortion-aware sparse adversarial attack. 2020.

Dugas, C., Bengio, Y., Bélisle, F., Nadeau, C., and Garcia, R. Incorporating second-order functional knowledge for better option pricing. *Advances in neural information processing systems*, 13, 2000.

Feng, R., Mangaokar, N., Chen, J., Fernandes, E., Jha, S., and Prakash, A. Graphite: Generating automatic physical examples for machine-learning attacks on computer vision systems. In *2022 IEEE 7th European symposium on security and privacy (EuroS&P)*, pp. 664–683. IEEE, 2022.

Frank, M., Wolfe, P., et al. An algorithm for quadratic programming. *Naval research logistics quarterly*, 3(1-2): 95–110, 1956.

Frankle, J. and Carbin, M. The lottery ticket hypothesis: Finding sparse, trainable neural networks. In *International Conference on Learning Representations*, 2019. URL https://openreview.net/forum?id=rJl-b3RcF7.

Fu, Y., Yu, Q., Zhang, Y., Wu, S., Ouyang, X., Cox, D., and Lin, Y. Drawing robust scratch tickets: Subnetworks with inborn robustness are found within randomly initialized networks. *Advances in Neural Information Processing Systems*, 34:13059–13072, 2021.

Golgooni, Z., Saberi, M., Eskandar, M., and Rohban, M. H. Zerograd : Mitigating and explaining catastrophic overfitting in fgsm adversarial training. *ArXiv*, abs/2103.15476, 2021. URL https://api.semanticscholar.org/CorpusID:232404666.

Goodfellow, I. J., Shlens, J., and Szegedy, C. Explaining and harnessing adversarial examples. *Computer Science*, 2014.

Gowal, S., Rebuffi, S., Wiles, O., Stimberg, F., Calian, D. A., and Mann, T. A. Improving robustness using generated data. *CoRR*, abs/2110.09468, 2021.

Guo, C., Gardner, J. R., You, Y., Wilson, A. G., and Weinberger, K. Q. Simple black-box adversarial attacks. *ArXiv*, abs/1905.07121, 2019. URL https://api.semanticscholar.org/CorpusID:86541092.

He, K., Zhang, X., Ren, S., and Sun, J. Deep residual learning for image recognition. In *Proceedings of the IEEE conference on computer vision and pattern recognition*, pp. 770–778, 2016a.

He, K., Zhang, X., Ren, S., and Sun, J. Identity mappings in deep residual networks. In *Computer Vision–ECCV 2016: 14th European Conference, Amsterdam, The Netherlands, October 11–14, 2016, Proceedings, Part IV 14*, pp. 630–645. Springer, 2016b.

Ilyas, A., Engstrom, L., Athalye, A., and Lin, J. Black-box adversarial attacks with limited queries and information. In *International Conference on Machine Learning*, 2018a. URL https://api.semanticscholar.org/CorpusID:5046541.

Ilyas, A., Engstrom, L., and Madry, A. Prior convictions: Black-box adversarial attacks with bandits and priors. *ArXiv*, abs/1807.07978, 2018b. URL https://api.semanticscholar.org/CorpusID:49907212.

Imtiaz, T., Kohler, M., Miller, J., Wang, Z., Sznaier, M., Camps, O., and Dy, J. Saif: Sparse adversarial and interpretable attack framework. *arXiv preprint arXiv:2212.07495*, 2022.

Jiang, Y., Liu, C., Huang, Z., Salzmann, M., and Süsstrunk, S. Towards stable and efficient adversarial training against l_1 bounded adversarial attacks. In *International Conference on Machine Learning*. PMLR, 2023.

Kang, P. and Moosavi-Dezfooli, S.-M. Understanding catastrophic overfitting in adversarial training. *ArXiv*, abs/2105.02942, 2021. URL https://api.semanticscholar.org/CorpusID:234093560.

Kim, H., Lee, W., and Lee, J. Understanding catastrophic overfitting in single-step adversarial training. In *AAAI Conference on Artificial Intelligence*, 2020. URL https://api.semanticscholar.org/CorpusID:222133879.

Krizhevsky, A., Hinton, G., et al. Learning multiple layers of features from tiny images. 2009.

Kurakin, A., Goodfellow, I., and Bengio, S. Adversarial examples in the physical world. 2016.

Kurakin, A., Goodfellow, I. J., and Bengio, S. Adversarial machine learning at scale. In *International Conference on Learning Representations*, 2017. URL https://openreview.net/forum?id=BJm4T4Kgx.

Liu, C., Zhao, Z., Süsstrunk, S., and Salzmann, M. Robust binary models by pruning randomly-initialized networks. *Advances in Neural Information Processing Systems*, 35: 492–506, 2022.

Madry, A., Makelov, A., Schmidt, L., Tsipras, D., and Vladu, A. Towards deep learning models resistant to adversarial attacks. *arXiv preprint arXiv:1706.06083*, 2017.

Meunier, L., Atif, J., and Teytaud, O. Yet another but more efficient black-box adversarial attack: tiling and evolution strategies. *ArXiv*, abs/1910.02244, 2019. URL https://api.semanticscholar.org/CorpusID:203837562.

Modas, A., Moosavi-Dezfooli, S. M., and Frossard, P. Sparsefool: a few pixels make a big difference. 2018.

Moon, S., An, G., and Song, H. O. Parsimonious black-box adversarial attacks via efficient combinatorial optimization. *ArXiv*, abs/1905.06635, 2019. URL https://api.semanticscholar.org/CorpusID:155100229.

Papernot, N., McDaniel, P., Goodfellow, I., Jha, S., Celik, Z. B., and Swami, A. Practical black-box attacks against machine learning. In *Proceedings of the 2017 ACM on Asia conference on computer and communications security*, pp. 506–519, 2017.

Rade, R. and Moosavi-Dezfooli, S.-M. Helper-based adversarial training: Reducing excessive margin to achieve a better accuracy vs. robustness trade-off. In *ICML 2021 Workshop on Adversarial Machine Learning*, 2021. URL https://openreview.net/forum?id=BuD2LmNaU3a.

Ramanujan, V., Wortsman, M., Kembhavi, A., Farhadi, A., and Rastegari, M. What's hidden in a randomly weighted neural network? In *Proceedings of the IEEE/CVF conference on computer vision and pattern recognition*, pp. 11893–11902, 2020.

Rebuffi, S., Gowal, S., Calian, D. A., Stimberg, F., Wiles, O., and Mann, T. A. Fixing data augmentation to improve adversarial robustness. *CoRR*, abs/2103.01946, 2021.

Sehwag, V., Mahloujifar, S., Handina, T., Dai, S., Xiang, C., Chiang, M., and Mittal, P. Robust learning meets generative models: Can proxy distributions improve adversarial robustness? *arXiv preprint arXiv:2104.09425*, 2021.

Shafahi, A., Najibi, M., Ghiasi, A., Xu, Z., Dickerson, J. P., Studer, C., Davis, L. S., Taylor, G., and Goldstein, T. Adversarial training for free! In *Neural Information Processing Systems*, 2019. URL https://api.semanticscholar.org/CorpusID:139102395.

Sriramanan, G., Addepalli, S., Baburaj, A., and Babu, R. V. Towards efficient and effective adversarial training. In *Neural Information Processing Systems*, 2021. URL https://api.semanticscholar.org/CorpusID:245261076.

Stallkamp, J., Schlipsing, M., Salmen, J., and Igel, C. Man vs. computer: Benchmarking machine learning algorithms for traffic sign recognition. *Neural networks*, 32: 323–332, 2012.

Su, J., Vargas, D. V., and Sakurai, K. One pixel attack for fooling deep neural networks. *IEEE Transactions on Evolutionary Computation*, 23(5):828–841, 2019.

Szegedy, C., Zaremba, W., Sutskever, I., Bruna, J., Erhan, D., Goodfellow, I., and Fergus, R. Intriguing properties of neural networks. *Computer Science*, 2013.

Tramer, F. and Boneh, D. Adversarial training and robustness for multiple perturbations. *Advances in neural information processing systems*, 32, 2019.

Tu, C.-C., Ting, P.-S., Chen, P.-Y., Liu, S., Zhang, H., Yi, J., Hsieh, C.-J., and Cheng, S.-M. Autozoom: Autoencoder-based zeroth order optimization method for attacking black-box neural networks. In *AAAI Conference on Artificial Intelligence*, 2018. URL https://api.semanticscholar.org/CorpusID:44079102.

Uesato, J., O'Donoghue, B., van den Oord, A., and Kohli, P. Adversarial risk and the dangers of evaluating against weak attacks. *ArXiv*, abs/1802.05666, 2018. URL https://api.semanticscholar.org/CorpusID:3639844.

Wang, Z., Pang, T., Du, C., Lin, M., Liu, W., and Yan, S. Better diffusion models further improve adversarial training. *ArXiv*, abs/2302.04638, 2023. URL https://api.semanticscholar.org/CorpusID:256697167.

Wei, X., Huang, Y., Sun, Y., and Yu, J. Unified adversarial patch for cross-modal attacks in the physical world. In *Proceedings of the IEEE/CVF International Conference on Computer Vision*, pp. 4445–4454, 2023.

Weng, T.-W., Zhang, H., Chen, H., Song, Z., Hsieh, C.-J., Boning, D. S., Dhillon, I. S., and Daniel, L. Towards fast computation of certified robustness for relu networks. *ArXiv*, abs/1804.09699, 2018. URL https://api.semanticscholar.org/CorpusID:13750928.

Wong, E., Rice, L., and Kolter, J. Z. Fast is better than free: Revisiting adversarial training. *ArXiv*, abs/2001.03994, 2020. URL https://api.semanticscholar.org/CorpusID:210164926.

Xu, H., Ma, Y., Liu, H., Deb, D., Liu, H., Tang, J., and Jain, A. K. Adversarial attacks and defenses in images, graphs and text: A review. *International Journal of Automation and Computing*, 17:151 – 178, 2019. URL https://api.semanticscholar.org/CorpusID:202660800.

Zagoruyko, S. and Komodakis, N. Wide residual networks. *arXiv preprint arXiv:1605.07146*, 2016.

Zhang, D., Zhang, T., Lu, Y., Zhu, Z., and Dong, B. You only propagate once: Accelerating adversarial training via maximal principle. In *Neural Information Processing Systems*, 2019a. URL https://api.semanticscholar.org/CorpusID:146120969.

Zhang, H., Yu, Y., Jiao, J., Xing, E. P., Ghaoui, L. E., and Jordan, M. I. Theoretically principled trade-off between robustness and accuracy. *ArXiv*, abs/1901.08573, 2019b. URL https://api.semanticscholar.org/CorpusID:59222747.

Zhang, H., Yu, Y., Jiao, J., Xing, E. P., and Jordan, M. I. Theoretically principled trade-off between robustness and accuracy. 2019c.

A. Additional Experiments

A.1. Results of Different Sparsity Levels and Different Datasets

In this subsection, we present the robust accuracy on CIFAR-10 with the sparsity level $k = 10$ and $k = 15$, as well as those on CIFAR-100 with $k = 10$ in Table 8, 9 and 10, respectively. The observations with different sparsity levels and on different datasets are consistent with those in Table 1 and 2, which indicates the effectiveness of our method.

Table 8. Robust accuracy of various models on different attacks that generate l_0 bounded perturbations, where the sparsity level $k = 10$. The models are trained on **CIFAR-10** (Krizhevsky et al., 2009). Note that we report results of Sparse-RS (RS) with tuned hyperparameters, which outperforms its original version in (Croce et al., 2022). CornerSearch (CS) is evaluated on 1000 samples due to its high computational complexity.

Model	Network	Clean	Black-Box		White-Box					**sAA**
			CS	RS	SF	PGD$_0$	SAIF	**sPGD**$_{\text{proj}}$	**sPGD**$_{\text{unproj}}$	
Vanilla	RN-18	93.9	3.2	0.5	40.6	11.5	31.8	0.5	7.7	**0.5**
l_∞-adv. trained, $\epsilon = 8/255$										
GD	PRN-18	87.4	36.8	24.5	69.9	50.3	63.0	31.0	37.3	**23.2**
PORT	RN-18	84.6	36.7	27.5	70.7	46.1	62.6	31.0	36.2	**25.0**
DKL	WRN-28	92.2	40.9	25.0	71.9	54.2	64.6	32.6	38.8	**23.7**
DM	WRN-28	92.4	38.7	23.7	68.7	52.7	62.5	31.2	37.4	**22.6**
l_2-adv. trained, $\epsilon = 0.5$										
HAT	PRN-18	90.6	47.3	40.4	74.6	53.5	71.4	37.3	36.7	**34.5**
PORT	RN-18	89.8	46.8	37.7	74.2	50.4	70.9	33.7	33.0	**30.6**
DM	WRN-28	95.2	57.8	47.9	78.3	65.5	80.9	47.1	48.2	**43.1**
FDA	WRN-28	91.8	55.0	49.4	79.6	58.6	77.5	46.7	49.0	**43.8**
l_1-adv. trained, $\epsilon = 12$										
l_1-APGD	PRN-18	80.7	51.4	51.1	74.3	60.7	68.1	47.2	47.4	**45.9**
Fast-EG-l_1	PRN-18	76.2	49.7	48.0	69.7	56.7	63.2	44.7	45.0	**43.2**
l_0-adv. trained, $k = 10$										
PGD$_0$-A	PRN-18	85.8	20.7	16.1	77.1	66.1	68.7	33.5	36.2	**15.1**
PGD$_0$-T	PRN-18	90.6	22.1	14.0	85.2	72.1	76.6	37.9	44.6	**13.9**
sAT	PRN-18	86.4	61.0	57.4	84.1	82.0	81.1	78.2	77.6	**57.4**
sTRADES	PRN-18	89.8	74.7	71.6	88.8	87.7	86.9	85.9	84.5	**71.6**

A.2. Comparison under Different Iterations on CIFAR-100

Similar to the observation in Section 5.2, Figure 2 also indicates that our method can obtain a higher attack success rate than the strong black-box attack Sparse-RS (RS) when the query budget is limited. Compared with the observation in Figure 1, the efficiency of RS, which is based on heuristic random search, improves when the search space becomes smaller, i.e., smaller image space and lower sparsity level k.

A.3. Comparison under Different Sparsity Levels

In this subsection, we compare our method sPGD with RS attack. Specifically, we compare these two attacks under different sparsity levels, i.e., the values of k. We can observe from Figure 3 that RS attack shows slightly better performance only on the l_∞ model and when k is small. The search space for the perturbed features is relatively small when k is small, which facilitates heuristic black-box search methods like RS attack. As k increases, sPGD outperforms RS attack in all cases until both attacks achieve almost 100% attack success rate.

A.4. Iteration Numbers Needed to Successfully Generate Adversarial Samples

Figure 4 illustrates the distribution of the iteration numbers needed by sPGD and RS to successfully generate adversarial samples. For l_∞, l_2 and l_1 robust models, our proposed sPGD consumes distinctly fewer iteration numbers to successfully generate an adversarial sample than RS, the strongest black-box attack in Table 1, while maintaining a high attack success rate. Similar to the observations in Figure 1, the model trained by sTRADES suffers from gradient masking. However, RS still requires a large query budget to successfully generate an adversarial sample. This further demonstrates the efficiency of

Table 9. Robust accuracy of various models on different attacks that generate l_0 bounded perturbations, where the sparsity level $k = 15$. The models are trained on **CIFAR-10** (Krizhevsky et al., 2009). Note that we report results of Sparse-RS (RS) with tuned hyperparameters, which outperforms its original version in (Croce et al., 2022). CornerSearch (CS) is evaluated on 1000 samples due to its high computational complexity.

Model	Network	Clean	Black-Box		White-Box					**sAA**
			CS	RS	SF	PGD$_0$	SAIF	**sPGD**$_{\text{proj}}$	**sPGD**$_{\text{unproj}}$	
Vanilla	RN-18	93.9	1.6	0.0	25.3	2.1	12.0	0.0	0.0	**0.0**
l_∞-adv. trained, $\epsilon = 8/255$										
GD	PRN-18	87.4	30.5	12.2	61.1	36.0	51.3	17.1	24.3	**11.3**
PORT	RN-18	84.6	30.8	15.2	62.1	31.4	52.1	17.4	23.0	**13.0**
DKL	WRN-28	92.2	35.3	13.2	62.5	41.2	52.3	18.4	24.9	**12.1**
DM	WRN-28	92.4	34.8	12.6	57.9	38.5	49.4	17.9	24.0	**11.6**
l_2-adv. trained, $\epsilon = 0.5$										
HAT	PRN-18	90.6	38.9	23.5	65.3	35.4	60.2	19.0	18.6	**16.6**
PORT	RN-18	89.8	36.8	20.6	64.3	30.6	59.7	16.0	15.5	**13.8**
DM	WRN-28	95.2	48.5	27.7	68.2	47.5	70.9	25.0	26.7	**22.1**
FDA	WRN-28	91.8	47.8	31.1	71.8	40.1	68.2	28.0	31.4	**25.5**
l_1-adv. trained, $\epsilon = 12$										
l_1-APGD	PRN-18	80.7	41.3	36.5	70.3	50.5	62.3	30.4	31.3	**29.0**
Fast-EG-l_1	PRN-18	76.2	40.7	34.8	64.9	46.7	56.9	29.6	30.1	**28.0**
l_0-adv. trained, $k = 15$										
PGD$_0$-A	PRN-18	83.7	17.5	6.1	73.7	62.9	60.5	19.4	27.5	**5.6**
PGD$_0$-T	PRN-18	90.5	19.5	7.2	85.5	63.6	69.8	31.4	41.2	**7.1**
sAT	PRN-18	80.9	46.0	37.6	77.1	74.1	72.3	71.2	70.3	**37.6**
sTRADES	PRN-18	90.3	71.7	63.7	89.5	88.1	86.5	85.9	83.8	**63.7**

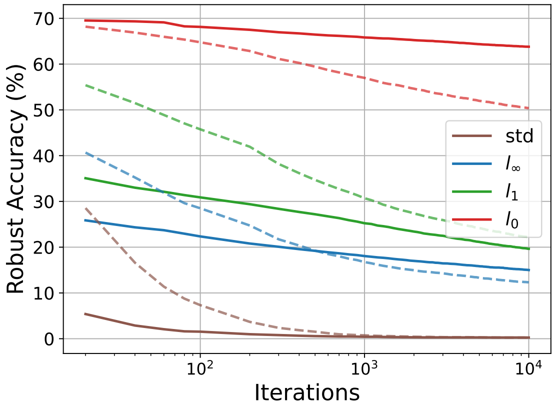

Figure 2. Comparison between sPGD and RS attack under different iterations on CIFAR-100 with $k = 10$. ResNet18 (std), FDA (l_∞) (Rebuffi et al., 2021), l_1-APGD (l_1) (Croce & Hein, 2021) and sTRADES (l_0) are evaluated. The total iteration number ranges from 20 and 10000. **The results of sPGD and RS attack are shown in solid lines and dotted lines, respectively.** For better visualization, the x-axis is shown in the log scale.

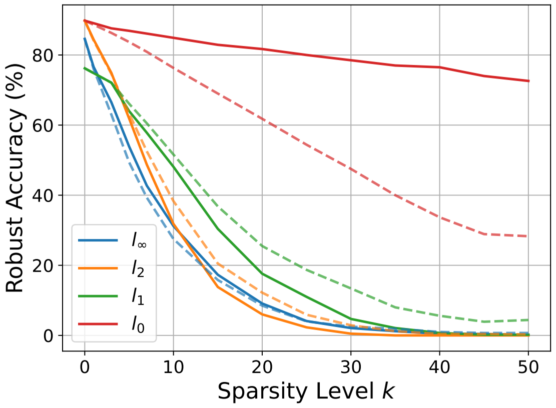

Figure 3. Comparison between sPGD and RS attack under different sparsity levels. PORT (l_∞ and l_2) (Sehwag et al., 2021), l_1-APGD (l_1) (Croce & Hein, 2021) and sTRADES (l_0) are evaluated. The k ranges from 0 and 50. The number of total iterations is set to 10000. **The results of sPGD and RS attack are shown in solid lines and dotted lines, respectively.**

sPGD, which makes it feasible for adversarial training.

A.5. More Ablation Study on sPGD

Step Size As shown in Table 11 and 12, the robust accuracy does not vary significantly with different step sizes. It indicates the satisfying robustness of our method to different hyperparameter choices. In practice, We set α and β to 0.25 and

Table 10. Robust accuracy of various models on different attacks that generate l_0 bounded perturbations, where the sparsity level $k = 10$. The models are trained on **CIFAR-100** (Krizhevsky et al., 2009). Note that we report results of Sparse-RS (RS) with tuned hyperparameters, which outperforms its original version in (Croce et al., 2022). CornerSearch (CS) is evaluated on 1000 samples due to its high computational complexity.

Model	Network	Clean	Black-Box		White-Box					sAA
			CS	RS	SF	PGD_0	SAIF	**sPGD**$_{\text{proj}}$	**sPGD**$_{\text{unproj}}$	
Vanilla	RN-18	74.3	1.6	0.3	20.1	1.9	9.0	0.1	0.9	**0.1**
l_∞-adv. trained, $\epsilon = 8/255$										
HAT	PRN-18	61.5	12.6	9.3	39.1	19.1	26.8	11.6	14.2	**8.5**
FDA	PRN-18	56.9	16.3	12.3	42.2	23.0	30.7	14.9	17.8	**11.6**
DKL	WRN-28	73.8	12.4	6.3	44.9	20.9	26.5	10.5	14.0	**6.1**
DM	WRN-28	72.6	14.0	8.2	46.2	23.4	29.8	12.7	15.8	**8.0**
l_1-adv. trained, $\epsilon = 6$										
l_1-APGD	PRN-18	63.2	22.7	22.1	47.7	33.0	43.5	19.7	20.3	**18.5**
Fast-EG-l_1	PRN-18	59.4	21.5	21.0	44.8	30.6	39.5	18.9	18.6	**17.3**
l_0-adv. trained, $k = 10$										
PGD_0-A	PRN-18	66.1	9.3	7.1	57.9	29.9	39.5	13.9	20.4	**6.5**
PGD_0-T	PRN-18	70.7	14.8	10.5	63.5	46.3	51.7	24.5	28.6	**10.2**
sAT	PRN-18	67.0	44.3	41.6	65.9	61.6	60.9	56.8	58.0	**41.6**
sTRADES	PRN-18	70.9	52.8	50.3	69.2	67.2	65.2	64.0	63.7	**50.2**

$0.25 \times \sqrt{h \times w}$, respectively. Note that h and w denote the height and width of the image, respectively, which are both 32 in CIFAR-10.

Tolerance during Attacking As shown in Table 13, the performance of our method remains virtually unchanged, which showcases that our approach is robust to different choices of tolerance for reinitialization.

Table 11. Robust accuracy at different step sizes α for magnitude p. The evaluated attack is $\text{sPGD}_{\text{proj}}$. The model is Fast-EG-$l_1$ (Jiang et al., 2023) trained on CIFAR-10 (Krizhevsky et al., 2009).

α	$\frac{1}{16}$	$\frac{1}{8}$	$\frac{1}{4}$	$\frac{1}{2}$	$\frac{3}{4}$	1
Acc.	19.6	18.8	**18.1**	18.4	18.7	19.0

Table 12. Robust accuracy at different step sizes β for mask m. The evaluated attack is $\text{sPGD}_{\text{proj}}$. The model is Fast-EG-$l_1$ (Jiang et al., 2023) trained on CIFAR-10 (Krizhevsky et al., 2009).

β	2	4	8	16	24	32
Acc.	20.0	19.3	**18.1**	18.4	19.4	21.0

A.6. Impact of Tolerance during Adversarial Training

We also study the impact of different tolerances for reinitialization during adversarial training. The results reported in Table 14 indicate that higher tolerance during adversarial training significantly improves the model's robustness against sparse attacks, and the performance reaches its best when the tolerance is set to 10.

Table 13. Robust accuracy at different tolerance for reinitialization t during attacking. The evaluated attack is $\text{sPGD}_{\text{proj}}$. The model is Fast-EG-$l_1$ (Jiang et al., 2023) trained on CIFAR-10 (Krizhevsky et al., 2009).

t	1	3	5	7	10
Acc.	18.1	**18.1**	18.5	18.5	18.5

Table 14. Ablation study on tolerance for reinitialization t during adversarial training. The model is PRN18 trained by sTRADES with $6 \times k$ and tolerance $t = 3$. The robust accuracy is obtained through sAA.

t	3	10	20
Acc.	51.7	**61.7**	60.0

B. Implementation Details

In experiments, we mainly focus on the cases of the sparsity of perturbations $k = 10, 15$ and 20, where $k = ||\sum_{i=1}^{c} \boldsymbol{\delta}^{(i)}||_0$ or $||\boldsymbol{m}||_0$, $\boldsymbol{\delta}^{(i)} \in \mathbb{R}^{h \times w}$ is the i-th channel of perturbation $\boldsymbol{\delta} \in \mathbb{R}^{h \times w \times c}$, and $\boldsymbol{m} \in \mathbb{R}^{h \times w \times 1}$ is the sparsity mask in the decomposition of $\boldsymbol{\delta} = \boldsymbol{p} \odot \boldsymbol{m}$, $\boldsymbol{p} \in \mathbb{R}^{h \times w \times c}$ denotes the magnitude of perturbations.

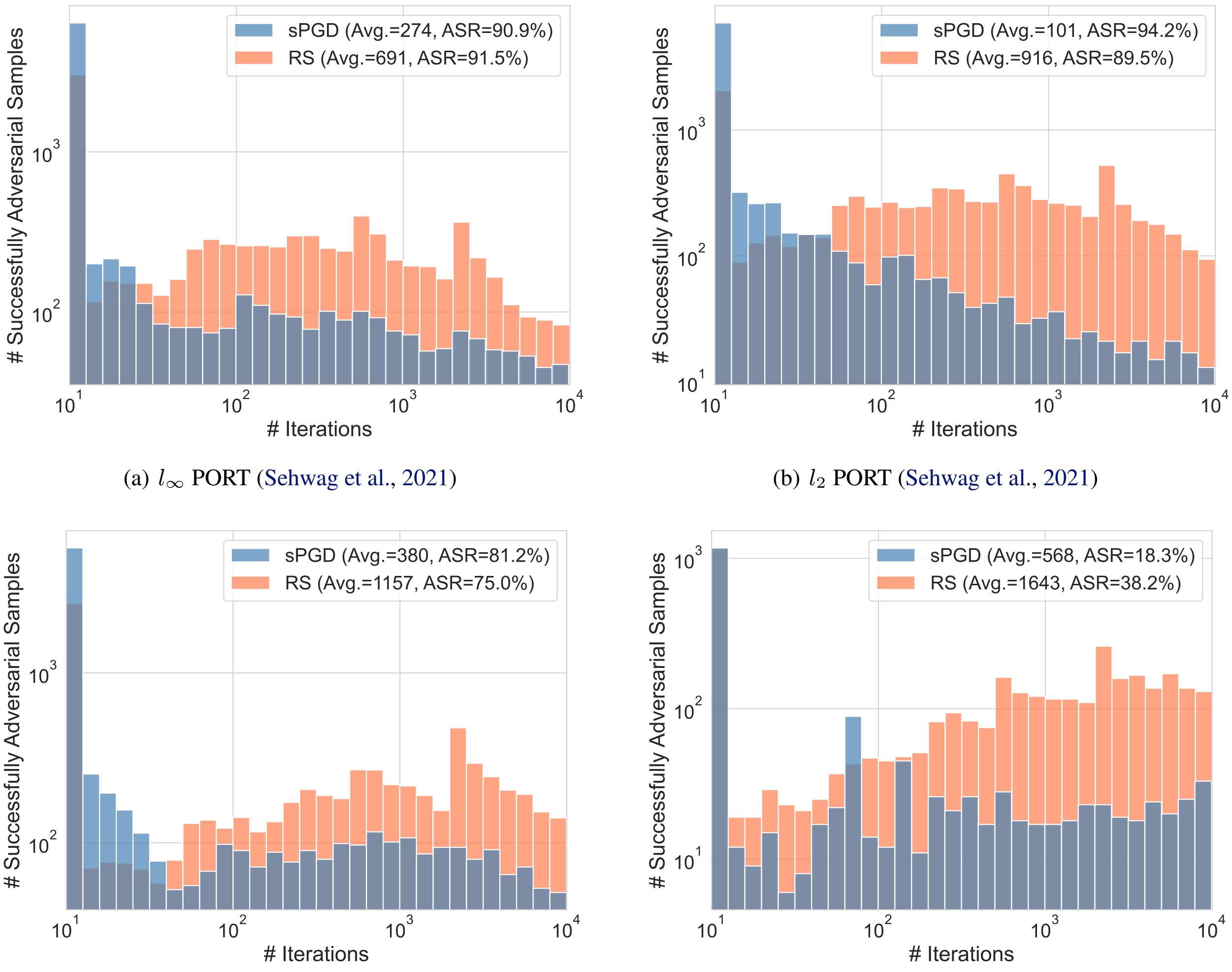

(a) l_∞ PORT (Sehwag et al., 2021)

(b) l_2 PORT (Sehwag et al., 2021)

(c) l_1-APGD (Croce & Hein, 2021)

(d) sTRADES

Figure 4. Distribution of the iteration numbers needed by sPGD (blue) and RS (orange) to successfully generate adversarial samples. The results are obtained from different models: **(a)** l_∞ PORT (Sehwag et al., 2021), **(b)** l_2 PORT (Sehwag et al., 2021), **(c)** l_1-APGD (Croce & Hein, 2021) and **(d)** our sPGD. The average iteration numbers (Avg.) and attack success rate (ASR), i.e., $1-$Robust Acc., are reported in the legend. For better visualization, we clip the minimum iteration number to 10 and show the x- and y-axis in log scale.

To exploit the strength of these attacks in reasonable running time, we run all these attacks for either 10000 iterations or the number of iterations where their performances converge. More details are elaborated below.

CornerSearch (Croce & Hein, 2019b): For CornerSearch, we set the hyperparameters as following: $N = 100, N_{iter} = 3000$, where N is the sample size of the one-pixel perturbations, N_{iter} is the number of queries. For bot CIFAR-10 and CIFAR-100 datasets, we evaluate the robust accuracy on 1000 test instances due to its prohibitively high computational complexity.

Sparse-RS (Croce et al., 2022): For Sparse-RS, we set $\alpha_{\text{init}} = 0.8$, which controls the set of pixels changed in each iteration. Cross-entropy loss is adopted. Following the default setting in (Croce et al., 2022), we report the results of untargeted attacks with the maximum queries up to 10000.

SparseFool (Modas et al., 2018): We apply SparseFool following the official implementation and use the default value of the sparsity parameter $\lambda = 3$. The maximum iterations per sample is set to 3000. Finally, the perturbation generated by SparseFool is projected to the l_0 ball to satisfy the adversarial budget.

PGD$_\mathbf{0}$ (Croce & Hein, 2019b): For PGD$_0$, we include both untargeted attack and targeted attacks on the top-9 incorrect classes with the highest confidence scores. We set the step size to $\eta = 120000/255$. Contrary to the default setting, the iteration numbers of each attack increase from 20 to 300. Besides, 5 restarts are adopted to boost the performance further.

SAIF (Imtiaz et al., 2022): Similar to PGD_0, we apply both untargeted attack and targeted attacks on the top-9 incorrect classes with 300 iterations per attack, however, the query budget is only 100 iterations in the original paper (Imtiaz et al., 2022). We adopt the same l_∞ norm constraint for the magnitude tensor p as in sPGD.

sparse-PGD (sPGD): Cross-entropy loss is adopted as the loss function of both untargeted and targeted versions of our method. The step size for magnitude $\boldsymbol{p}$ is set $\alpha = 1/4$; the step size for continuous mask $\widetilde{\boldsymbol{m}}$ is set $\beta = 1/4 \times \sqrt{h \times w}$, where h and w are the height and width of the input image $\boldsymbol{x} \in \mathbb{R}^{h \times w \times c}$, respectively. The small constant γ to avoid numerical error is set to 1×10^{-10}. The number of iterations is 10000 for all datasets to ensure fair comparison among attacks in Table 1. The tolerance for reinitialization is set to 3.

sparse-AutoAttack (sAA): It is a cascade ensemble of five different attacks, i.e., **a)** untargeted sPGD with unprojected gradient ($\text{sPGD}_{\text{unproj}}$), **b)** untargeted sPGD with sparse gradient ($\text{sPGD}_{\text{proj}}$), and **c)** untargeted Sparse-RS. The hyper-parameters of sPGD are the same as those listed in the last paragraph.

Adversarial Training: sPGD is adopted as the attack during the training phase, the number of iterations is 20, and the backward function is randomly selected from the two different backward functions for each batch. For sTRADES, we only compute the TRADES loss when training, and generating adversarial examples is based on cross-entropy loss. We use PreactResNet18 (He et al., 2016b) with softplus activation (Dugas et al., 2000) for experiments on CIFAR-10 and CIFAR-100 (Krizhevsky et al., 2009), and ResNet34 (He et al., 2016a) for experiments on ImageNet100 (Deng et al., 2009) and GTSRB (Stallkamp et al., 2012). We train the model for 100 epochs on CIFAR-10 and CIFAR-100, for 40 epochs on ImageNet100, and for 20 epochs on GTSRB. The training batch size is 128 on CIFAR-10 and CIFAR-100, and 32 on ImageNet100 and GTSRB. The optimizer is SGD with a momentum factor of 0.9 and weight decay factor of 5×10^{-4}. The learning rate is initialized to 0.05 and is divided by a factor of 10 at the $\frac{1}{4}$ and the $\frac{3}{4}$ of the total epochs. The tolerance for reinitialization is set to 10.

C. Visualization of Some Adversarial Samples

We show some adversarial examples with different sparsity levels of perturbation in Figure 5, 6, 7. The attack is sPGD, and the model is Fast-EG-l_1 (Jiang et al., 2023) trained on CIFAR-10. We can observe that most of the perturbed pixels are located in the foreground of images. It is consistent with the intuition that the foreground of an image contains most of the semantic information.

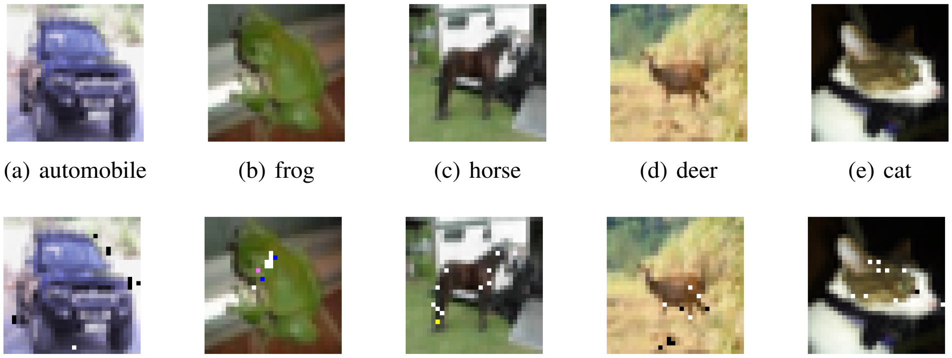

(a) automobile (b) frog (c) horse (d) deer (e) cat

(f) truck (g) deer (h) automobile (i) bird (j) ship

Figure 5. Clean images (first row) from the test set of CFIFAR-10 and their corresponding adversarial samples (second row) by sPGD. The attack is sPGD with sparsity level $k = 10$. The model is Fast-EG-l_1 trained on CIFAR-10. The predictions given by the model are listed below the images.

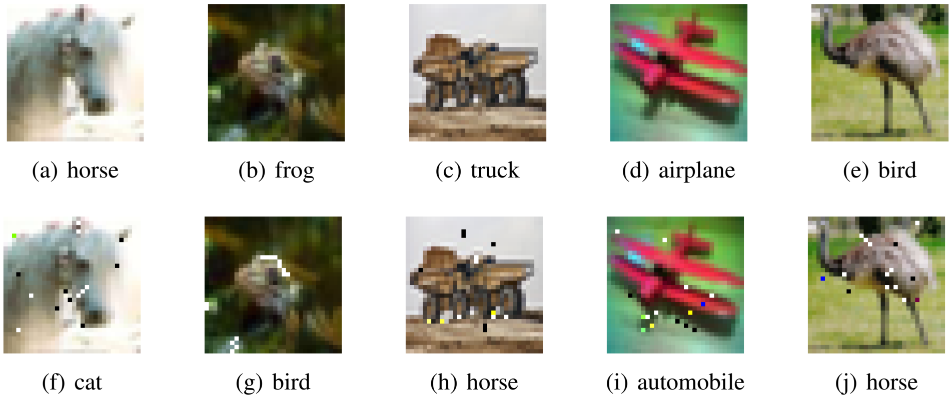

(a) horse (b) frog (c) truck (d) airplane (e) bird

(f) cat (g) bird (h) horse (i) automobile (j) horse

Figure 6. Clean images (first row) from the test set of CFIFAR-10 and their corresponding adversarial samples (second row) by sPGD. The attack is sPGD with sparsity level $k = 15$. The model is Fast-EG-l_1 trained on CIFAR-10. The predictions given by the model are listed below the images.

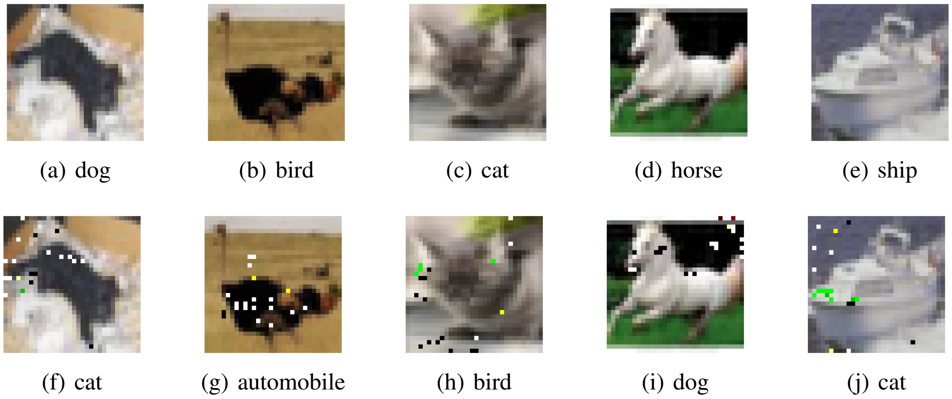

(a) dog (b) bird (c) cat (d) horse (e) ship

(f) cat (g) automobile (h) bird (i) dog (j) cat

Figure 7. Clean images (first row) from the test set of CFIFAR-10 and their corresponding adversarial samples (second row) by sPGD. The attack is sPGD with sparsity level $k = 20$. The model is Fast-EG-l_1 trained on CIFAR-10. The predictions given by the model are listed below the images.